

1 This document was prepared as an account of work sponsored by the United States Government. While  
2 this document is believed to contain correct information, neither the United States Government nor any  
3 agency thereof, nor the Regents of the University of California, nor any of their employees, makes any  
4 warranty, express or implied, or assumes any legal responsibility for the accuracy, completeness, or  
5 usefulness of any information, apparatus, product, or process disclosed, or represents that its use would  
6 not infringe privately owned rights. Reference herein to any specific commercial product, process, or  
7 service by its trade name, trademark, manufacturer, or otherwise, does not necessarily constitute or imply  
8 its endorsement, recommendation, or favoring by the United States Government or any agency thereof, or  
9 the Regents of the University of California. The views and opinions of authors expressed herein do not  
10 necessarily state or reflect those of the United States Government or any agency thereof or the Regents of  
11 the University of California.

12

13 **Characterization of Electrode Materials for Lithium Ion and Sodium Ion Batteries using**

14 **Synchrotron Radiation Techniques**

15 Marca M. Doeff  
16 Environmental Energy Technologies Division  
17 Lawrence Berkeley National Laboratory  
18 University of California  
19 Berkeley, CA 94720 USA  
20 [mmdoeff@lbl.gov](mailto:mmdoeff@lbl.gov)  
21 510 486-5821

22  
23 Guoying Chen  
24 Environmental Energy Technologies Division  
25 Lawrence Berkeley National Laboratory  
26 [GChen@lbl.gov](mailto:GChen@lbl.gov)

27  
28 Jordi Cabana  
29 Environmental Energy Technologies Division  
30 Lawrence Berkeley National Laboratory  
31 [JCabana@lbl.gov](mailto:JCabana@lbl.gov)

32  
33 Thomas J. Richardson  
34 Environmental Energy Technologies Division  
35 Lawrence Berkeley National Laboratory

36  
37 Apurva Mehta  
38 Stanford Synchrotron Radiation Lightsource  
39 2575 Sand Hill Road  
40 Menlo Park, CA 94025  
41 [mehta@slac.stanford.edu](mailto:mehta@slac.stanford.edu)

42  
43 Mona Shirpour  
44 Environmental Energy Technologies Division  
45 Lawrence Berkeley National Laboratory  
46 [MShirpour@lbl.gov](mailto:MShirpour@lbl.gov)

47  
48 Hugues Duncan  
49 Environmental Energy Technologies Division  
50 Lawrence Berkeley National Laboratory  
51 [HDuncan@lbl.gov](mailto:HDuncan@lbl.gov)

52  
53 Chunjoong Kim  
54 Environmental Energy Technologies Division  
55 Lawrence Berkeley National Laboratory  
56 [ckim@lbl.gov](mailto:ckim@lbl.gov)

57  
58  
59 Kinson C. Kam  
60 Haldor Topsøe A/S  
61 Nymoellevej 55  
62 2800 Kgs. Lyngby  
63 Denmark  
64 [kcka@topsoe.dk](mailto:kcka@topsoe.dk)

65  
66 Thomas Conry  
67 PolyPlus Battery Company  
68 2424 6th St, Berkeley, CA 94710  
69 Thomas.Conry@gmail.com

70  
71 **Corresponding author**

72 Marca M. Doeff

73  
74 **Keywords**

75  
76 Electrode materials, Li ion battery, Na ion battery, X-ray Absorption Spectroscopy (XAS), *in*  
77 *situ* X-ray diffraction (XRD)

78  
79 **Short Abstract**

80  
81 We describe the use of synchrotron X-ray absorption spectroscopy (XAS) and X-ray diffraction  
82 (XRD) techniques to probe details of intercalation/deintercalation processes in electrode  
83 materials for Li ion and Na ion batteries. Both *in situ* and *ex situ* experiments are used to  
84 understand structural behavior relevant to the operation of devices.

85  
86 **Long Abstract**

87  
88 Intercalation compounds such as transition metal oxides or phosphates are the most commonly  
89 used electrode materials in Li-ion and Na-ion batteries. During insertion or removal of alkali  
90 metal ions, the redox states of transition metals in the compounds change and structural  
91 transformations such as phase transitions and/or lattice parameter increases or decreases occur.  
92 These behaviors in turn determine important characteristics of the batteries such as the potential  
93 profiles, rate capabilities, and cycle lives. The extremely bright and tunable x-rays produced by  
94 synchrotron radiation allow rapid acquisition of high-resolution data that provide information  
95 about these processes. Transformations in the bulk materials, such as phase transitions, can be  
96 directly observed using X-ray diffraction (XRD), while X-ray absorption spectroscopy (XAS)  
97 gives information about the local electronic and geometric structures (e.g., changes in redox  
98 states and bond lengths). *In situ* experiments carried out on operating cells are particularly useful  
99 because they allow direct correlation between the electrochemical and structural properties of the  
100 materials. These experiments are time-consuming and can be challenging to design due to the  
101 reactivity and air-sensitivity of the alkali metal anodes used in the half-cell configurations, and/or  
102 the possibility of signal interference from other cell components and hardware. For these

103 reasons, it is appropriate to carry out *ex situ* experiments (e.g., on electrodes harvested from  
104 partially charged or cycled cells) in some cases. Here, we present detailed protocols for the  
105 preparation of both *ex situ* and *in situ* samples for experiments involving synchrotron radiation  
106 and demonstrate how these experiments are done.

107

## 108 **Introduction**

109

110 Lithium ion batteries for consumer electronics presently command an \$11 billion market  
111 worldwide ([http://www.marketresearch.com/David-Company-v3832/Lithium-Ion-Batteries-](http://www.marketresearch.com/David-Company-v3832/Lithium-Ion-Batteries-Outlook-Alternative-6842261/)  
112 [Outlook-Alternative-6842261/](http://www.marketresearch.com/David-Company-v3832/Lithium-Ion-Batteries-Outlook-Alternative-6842261/)) and are the premier choice for emerging vehicular applications  
113 such as plug-in hybrid electric vehicles (PHEVs) and electric vehicles (EVs). Analogs to these  
114 devices utilizing sodium ions rather than lithium are in earlier stages of development, but are  
115 considered attractive for large scale energy storage (i.e., grid applications) based on cost and  
116 supply security arguments.<sup>1,2</sup> Both dual intercalation systems work on the same principle; alkali  
117 metal ions shuttle between two electrodes acting as host structures, which undergo insertion  
118 processes at different potentials. The electrochemical cells themselves are relatively simple,  
119 consisting of composite positive and negative electrodes on current collectors, separated by a  
120 porous membrane saturated with an electrolytic solution usually consisting of a salt dissolved in  
121 a mixture of organic solvents (Figure 1). Graphite and LiCoO<sub>2</sub> are the most commonly employed  
122 negative and positive electrodes, respectively, for lithium ion batteries. Several alternative  
123 electrode materials have also been developed for specific applications, including variants of  
124 LiMn<sub>2</sub>O<sub>4</sub> spinel, LiFePO<sub>4</sub> with the olivine structure, and NMCs (LiNi<sub>x</sub>Mn<sub>x</sub>Co<sub>1-2x</sub>O<sub>2</sub> compounds)  
125 for positives, and hard carbons, Li<sub>4</sub>Ti<sub>5</sub>O<sub>12</sub>, and alloys of lithium with tin for negatives.<sup>3</sup> High  
126 voltage materials like LiNi<sub>0.5</sub>Mn<sub>1.5</sub>O<sub>4</sub>, new high capacity materials such as layered-layered  
127 composites (e.g., xLi<sub>2</sub>MnO<sub>3</sub>·(1-x)LiMn<sub>0.5</sub>Ni<sub>0.5</sub>O<sub>2</sub>), compounds with transition metals that can  
128 undergo multiple changes in redox states, and Li-Si alloy anodes are currently subjects of intense  
129 research, and, if successfully deployed, should raise practical energy densities of lithium ion cells  
130 further. Another class of materials, known as conversion electrodes, in which transition metal  
131 oxides, sulfides, or fluorides are reversibly reduced to the metallic element and a lithium salt, are  
132 also under consideration for use as battery electrodes (primarily as replacements for anodes).<sup>4</sup>  
133 For devices based on sodium, hard carbons, alloys, Nasicon structures, and titanates are being  
134 investigated for use as anodes and various transition metal oxides and polyanionic compounds as  
135 cathodes.

136 Because lithium ion and sodium ion batteries are not based on fixed chemistries, their  
137 performance characteristics vary considerably depending on the electrodes that are employed.  
138 The redox behavior of the electrodes determines the potential profiles, rate capabilities, and cycle  
139 lives of the devices. Conventional powder x-ray diffraction (XRD) techniques can be used for  
140 initial structural characterization of pristine materials and *ex situ* measurements on cycled  
141 electrodes, but practical considerations such as low signal strength and the relatively long times  
142 needed to collect data limit the amount of information that can be obtained on the discharge and  
143 charge processes. In contrast, the high brilliance and short wavelengths of synchrotron radiation  
144 (e.g.,  $\lambda=0.97$  Å at the Stanford Synchrotron Radiation Lightsource's beamline 11-3), combined  
145 with the use of high throughput image detectors, permit acquisition of high-resolution data on  
146 samples in as little as 10 seconds. *In situ* work is performed in transmission mode on cell  
147 components undergoing charge and discharge in hermetically sealed pouches transparent to x-  
148 rays, without having to stop operation to acquire data. As a result, electrode structural changes

149 can be observed as “snapshots in time” as the cell cycles, and much more information can be  
150 obtained than with conventional techniques.

151  
152 X-ray absorption spectroscopy (XAS), also sometimes referred to as X-ray Absorption Fine  
153 Structure (XAFS) gives information about the local electronic and geometric structure of  
154 materials. In XAS experiments, the photon energy is tuned to the characteristic absorption edges  
155 of the specific elements under investigation. Most commonly for battery materials, these energies  
156 correspond to the K-edges (1s orbitals) of the transition metals of interest, but soft XAS  
157 experiments tuned to O, F, C, B, N and the L<sub>2,3</sub> edges of first row transition metals are also  
158 sometimes carried out on *ex situ* samples.<sup>5</sup> The spectra generated by XAS experiments can be  
159 divided into several distinct regions, containing different information (see Newville, M.,  
160 Fundamentals of XAFS.

161 [http://xafs.org/Tutorials?action=AttachFile&do=get&target=Newville\\_xas\\_fundamentals.pdf](http://xafs.org/Tutorials?action=AttachFile&do=get&target=Newville_xas_fundamentals.pdf).  
162 The main feature, consisting of the absorption edge and extending about 30-50 eV beyond is the  
163 X-ray Absorption Near Edge Structure (XANES) region and indicates the ionization threshold to  
164 continuum states. This contains information about the oxidation state and coordination  
165 chemistry of the absorber. The higher energy portion of the spectrum is known as the Extended  
166 X-ray Absorption Fine Structure (EXAFS) region and corresponds to the scattering of the ejected  
167 photoelectron off neighboring atoms. Fourier analysis of this region gives short-range structural  
168 information such as bond lengths and the numbers and types of neighboring ions. Pre-edge  
169 features below the characteristic absorption energies of some compounds also sometimes appear.  
170 These arise from dipole forbidden electronic transitions to empty bound states **for octahedral**  
171 **geometries, or dipole allowed orbital hybridization effects in tetrahedral ones** and can often be  
172 correlated to the local symmetry of the absorbing ion (e.g., whether it is tetrahedrally or  
173 octahedrally coordinated).<sup>6</sup>

174 XAS is a particularly useful technique for studying mixed metal systems such as NMCs to  
175 determine initial redox states and which transition metal ions undergo redox during delithiation  
176 and lithiation processes. Data on several different metals can be obtained rapidly in a single  
177 experiment and interpretation is reasonably straightforward. In contrast, Mossbauer spectroscopy  
178 is limited to only a few metals used in battery materials (primarily, Fe and Sn). While magnetic  
179 measurements can also be used to determine oxidation states, magnetic coupling effects can  
180 complicate interpretation particularly for complex oxides such as the NMCs.

181 Well-planned and -executed *in situ* and *ex situ* synchrotron XRD and XAS experiments give  
182 complementary information and allow a **more** complete picture to be formed of the structural  
183 changes occurring in electrode materials during normal battery operation **than what can be**  
184 **obtained via conventional techniques**. This, in turn, gives a greater understanding of what  
185 governs the electrochemical behavior of the devices.

## 186 Protocol

187

### 188 1. Planning of Experiments

189 1.1 Identify beam line experiments of interest. Refer to beam line webpages as guides. For  
190 SSRL XAS and XRD, these are: <http://www-ssrl.slac.stanford.edu/beamlines/bl4-1/> and

191 <http://www-ssrl.slac.stanford.edu/beamlines/bl4-3/> and [http://www-](http://www-ssrl.slac.stanford.edu/beamlines/bl11-3/)  
192 [ssrl.slac.stanford.edu/beamlines/bl11-3/](http://www-ssrl.slac.stanford.edu/beamlines/bl11-3/)

193 1.1.1 Contact beam line scientist and discuss details of experiment.

194 1.2. Check deadlines and requirements for proposals by going to the relevant website.

195 1.3. Write beam time proposal and submit.

196 1.4. After the proposal has been scored, schedule beam time.

197 1.5. Follow instructions provided by the facility to prepare for beam time. Consider the details  
198 of the experiment, transport of materials (especially of devices containing alkali metals) and  
199 equipment, and any safety concerns. Safety training is generally required for new users.

## 200 **2. Preparation of Materials, Electrodes, and Cells**

201 2.1. Synthesize or obtain active material of interest.

202 2.2. Characterize material by conventional x-ray powder diffraction, using steps 2.2.1-2.2.9.

203 2.2.1. Grind powder and sieve to ensure uniform particle size distribution.

204 2.2.2. Load sample into sample holder. Remove backplate from holder and place it against a  
205 glass slide. Fill cavity with powder, then attach backplate, flip holder and remove slide. This  
206 ensures that the powder is even with the surface of the holder and that the surface is flat.

207 2.2.3. Log into logbook for the diffractometer.

208 2.2.4. Insert sample holder into diffractometer and align.

209 2.2.5. Close doors of diffractometer.

210 2.2.6. Using Data Collector program on computer attached to Panalytical diffractometer,  
211 increase voltage and current to values appropriate for measurement. Select slits and beam masks  
212 for the experiment. Select or modify program for scan.

213 2.2.7. Start program and name datafile. Lock diffractometer doors by swiping badge when  
214 prompted by the program. Collect data.

215 2.2.8. Analyze pattern using High Score program. In particular, look for the presence of  
216 impurities (extra reflections) and whether pattern matches that of reference materials or  
217 calculated patterns.

218 2.2.9. Remove sample from diffractometer. Turn down current and voltage, and close doors. Log  
219 out, noting any unusual conditions.

220 2.3. Obtain scanning electron micrographs to assess particle morphologies, using steps 2.3.1.-  
221 2.3.10.

222 2.3.1. Prepare sample by attaching carbon tape to an aluminum stub, and sprinkling sample  
223 powder onto sticky side. Test for magnetism by holding a kitchen magnet over the sample.

224 2.3.2. Insert sample into SEM chamber via airlock.

225 2.3.3. Once vacuum is established, turn accelerating voltage on.

226 2.3.4. In low magnification mode, adjust contrast and brightness. This is most conveniently done  
227 using the ACB button.

228 2.3.5. Find area of interest by manually scanning in the x and y directions.

229 2.3.6. Switch to SEM or gentle beam modes if higher magnification is desired. Select desired  
230 detector, and set working distance to values appropriate for the experiment.

231 2.3.7. Adjust contrast and brightness using ACB knob.

232 2.3.8. Focus image with stage z control.

233 2.3.8. Align beam, correct astigmatism and focus using x and y knobs.

234 2.3.9. Take pictures as desired, using photo button, and save to appropriate folder on the  
235 computer.

236 2.3.10. When finished, turn off accelerating voltage. Move sample to exchange position and  
237 remove from chamber via airlock.

238 2.4. Do elemental analysis by ICP if needed, and characterize materials with any other desired  
239 techniques such as IR or Raman spectroscopy.

240 2.5. Fabricate electrodes, using steps 2.5.1.-2.5.8.

241 2.5.1. Make a solution of 5-6 wt. % polyvinylidene fluoride (PVDF) in N-methylpyrrolidinone  
242 (NMP).

243 2.5.2. Mill together active material and conductive additive (acetylene black, graphite, etc.).

244 2.5.3. Add NMP solution from step 2.3.1 to dry powder from step 2.3.2 and mix. Proportions  
245 vary depending on the nature of the active material, but a final dry composition of 80:10:10  
246 (active material:PVDF:conductive additive) is common.

247 2.5.4. Using a doctor blade and (optionally) a vacuum table, cast electrode slurry onto an Al or  
248 Cu current collector. Carbon coated Al foil may be used for Li ion battery cathode materials and  
249 all Na ion electrode materials, and Cu foil is used for Li ion anode materials.

250 2.5.5. Allow electrodes to air-dry.

251 2.5.6. Dry electrodes further using an IR lamp, hot plate, or vacuum oven.

252 2.5.7. Cut or punch electrodes to the size needed. Weigh electrodes.

253 2.5.8. Transfer electrodes to an inert atmosphere glovebox. An additional drying step using a  
254 vacuum heated antechamber attached to the glovebox is recommended to remove all residual  
255 moisture.

256 2.6. Assemble electrochemical devices (usually coin cells, but other configurations can be  
257 used for electrochemical characterization) for initial characterization, *ex situ* samples, and/or  
258 beam line experiment, using steps 2.6.1-2.6.7.

259 2.6.1. Gather all needed components in the inert atmosphere glovebox.

260 2.6.2. Cut lithium or sodium foil to the desired size.

261 2.6.3. Cut microporous separator to the desired size.

262 2.6.4. Layer components in this order in the device: electrode, separator, electrolytic solution,  
263 and Li or Na foil.

264 2.6.5. Add spacers and wave washers as needed.

265 2.6.6. Seal cell using a coin cell press.

266 2.6.7. For *in situ* XRD experiments, attach tabs to either side of coin cell and seal device in  
267 polyester pouch.

268 2.7. Perform electrochemical experiment for initial characterization or *ex situ* work, using  
269 steps 2.7.1-2.7.6.

270 2.7.1. Connect leads from the potentiostat/galvanostat or cycler to device and measure open  
271 circuit potential.

272 2.7.2. Write program for the electrochemical experiment desired or select an archived program.

273 2.7.3. Run experiment and collect data.

274 2.7.4. For *ex situ* experiments, disassemble the device in glovebox, taking care not to short-  
275 circuit it. For coin cells, use either a coin cell disassembler tool or pliers wrapped with Teflon  
276 tape.

277 2.7.5. Rinse electrodes with dimethylcarbonate to remove residual electrolyte salt. Allow them  
278 to dry.

279 2.7.6. Cover electrodes for *ex situ* study with Kapton foil for XRD experiments or scotch tape  
280 for XAS and store in the glovebox until the experiment is carried out.

281 2.8. Powders intended for study by XAS should be sieved to ensure particle size  
282 homogeneity. They may then be sprinkled onto several pieces of scotch tape. A series of samples  
283 can then be prepared by stacking progressively more numerous pieces of the powdered tape  
284 together. This is particularly useful if the user is uncertain about the amount of powder needed  
285 for the optimal signal.

286 2.8.1. Alternatively, powders for XAS measurements may be diluted with BN if the user is  
287 confident about what will result in the optimum signal.

### 288 3. Performance of Experiments at the Synchrotron Facility

289 3.1. Several days before the experiment is to begin, plan transport of materials and equipment  
290 to the facility.

291 3.1.1. For devices containing alkali metal anodes, shipping is required to avoid hazards  
292 associated with transportation in personal or public vehicles.

293 3.1.2. Equipment such as portable galvanostat/potentiostats and laptop computers and  
294 nonhazardous samples such as electrodes for *ex situ* work may be brought to the facility by the  
295 individual carrying out the experiments in any convenient fashion.

296 3.2. Check in and register at the facility.

297 3.3 For both *in situ* and *ex situ* XRD experiments, take a reference pattern of LaB<sub>6</sub> for  
298 purposes of calibration.

299 3.3.1. Contact beamline scientist and personnel for instructions.

300 3.3.2. Calibrate beam to find right beam conditions.

301 3.3.3. Measure reference pattern of LaB<sub>6</sub>.

302 3.4. For *in situ* XRD experiments, set up device and start experiment following steps 3.4.1-  
303 3.4.6.

304 3.4.1. Insert pouch into Al pressure plates and ensure that holes are properly aligned to allow  
305 the x-ray beam to transmit.

306 3.4.2. Find optimum beam position and exposure time. Prolonged exposure can lead to  
307 oversaturation. Decide whether sample will be rocked or stationary.

308 3.4.3. Take initial pattern before electrochemistry is started.

309 3.4.4. Attach leads from galvanostat/potentiostat to device.

310 3.4.5. Start electrochemistry experiment.

311 3.4.6. Obtain data. Once experiment is under way, data collection is automatic, and user need  
312 only to oversee to make sure experiment is going as planned.

313 3.5. Set up XAS experiments.

314 3.5.1. Check in and contact beamline scientist and personnel for instructions.

315 3.5.2. Insert sample and foil reference material (depending on metal that is being measured;  
316 e.g., Ni for Ni K edge).

317 3.5.3. Align sample.

318 3.5.4. Determine energy of specific metal edge using IFEFFIT's Hephaestus. Tune  
319 monochromator, then de-tune by about 30% to eliminate higher order harmonics. Change gains  
320 to adjust  $I_1$  and  $I_2$  measure offsets.

321 3.5.5. Take measurement. Two or more scans should be taken and merged for the element of  
322 interest.

323 3.5.5. Repeat steps 3.5.3 to 3.5.5 for additional elements, as needed.

324 **4. Data analysis**

325 **4.1.** For XRD work, calibrate the LaB<sub>6</sub> image

326 **4.1.1.** Download Area Diffraction Machine, which is available through the google code  
327 (<http://code.google.com/p/areadiffractionmachine/>).

328 **4.1.2.** Open the image for LaB<sub>6</sub> diffraction and use initial calibration values from the file header

329 **4.1.3.** Open the reference  $Q (=2\pi/d)$  values of LaB<sub>6</sub>

330 **4.1.4.** Calibrate the LaB<sub>6</sub> diffraction image with the  $Q$  values and the initial guess of the  
331 calibration values.

332 **4.1.5.** Obtain correct calibration values by image fitting.

333 **4.1.6.** Save the calibration values into the calibration file.

334 **4.2.** Calibrate the data images from the experiment.

335 **4.2.1.** Open the diffraction images from the experiment.

336 **4.2.2.** Open the calibration file from the LaB<sub>6</sub> reference (saved in 4.1.6).

337 **4.2.3.** Open the reference  $Q (=2\pi/d)$  values of Al or Cu (current collectors for the electrodes)  
338 and use them as internal references.

339 **4.2.4.** Calibrate the pattern images by image fitting.

340 **4.2.5.** Integrate the image to  $Q$  vs. Intensity data (line scans).

341 **4.2.6.** Fit patterns using the desired fitting program (CelRef, Powdercell, RIQAS, GSAS, etc.).

342 **4.3.** Process electrochemical data using any convenient plotting program (Excel, Origin,  
343 KaleidaGraph, Igor, etc.).

344 **4.4.** For XAS data, use ARTEMIS/ATHENA in the IFEFFIT software package for analysis.

345 **4.4.1.** Calibrate data using the first peak in the derivative of the absorption spectra of the  
346 reference metals.

347 **4.4.2.** Merge like scans.

- 348 **4.4.3.** Subtract background and normalize data.
- 349 **4.4.4.** Use the AUTOBK function to isolate the EXAFS data.
- 350 **4.4.5.** Fourier transform the EXAFS data.
- 351 **4.4.6.** Use a least squares fit to the Fourier transformed spectra in R or k space to extract  
352 structural information.

### 353 **Representative Results**

354 Figure 2 shows a typical sequence used for an *in situ* experiment. After synthesis and  
355 characterization of active material powders, composite electrodes are prepared from slurries  
356 containing the active material, a binder such as polyvinylidene fluoride (PVDF) and conductive  
357 additives such as carbon black or graphite suspended in N-methylpyrrolidinone (NMP), cast onto  
358 either aluminum or copper foil current collectors. Aluminum is used for lithium ion battery  
359 cathodes and all sodium ion battery electrodes, and copper is used for lithium ion battery anodes.  
360 After the electrodes are dried, cut and weighed, cells are assembled in an inert atmosphere  
361 glovebox using microporous separators, the appropriate electrolytic solutions and negative  
362 electrodes consisting of either Li or Na foils. These components are then hermetically sealed in a  
363 protective pouch, made of polyester, which keeps out air and is reasonably x-ray transparent.  
364 Aluminum and nickel tabs are used to make electrical contacts to the positive and negative  
365 electrodes, respectively. The Al tabs are ultrasonically welded to the cathode current collectors,  
366 while the soft Li or Na metal used as the anode is simply pressed around the Ni tab to make  
367 contact. To maintain pressure, the pouch cell is compressed between two metal plates with 2 mm  
368 holes cut into them to allow the transmission of x-rays. Poor contact between cell components  
369 may result in high overpotentials and premature cutoff, particularly if voltage limits are not  
370 adjusted to accommodate the additional overpotential encountered in this configuration.  
371 Excessive pressure, on the other hand, may cause cell shorting and failure of the experiment.  
372 Better pressure control is achieved when components are first assembled into a coin cell with  
373 small holes drilled into the casings and spacers, which is then sealed into the protective pouch  
374 after tabs are attached. Wave washers and spacers are used to fill any extra volume in the device,  
375 maintain pressure, and ensure good contact among the components.

376 A small portable potentiostat/galvanostat and laptop computer are then used to perform the  
377 electrochemical experiment and collect data at the beam line. One charge-discharge cycle  
378 typically takes about 20 hours to complete. The cycle is usually performed galvanostatically (i.e.,  
379 using constant current) between pre-selected voltage limits. The sample may either be kept  
380 stationary, rocked (left/right or up/down) or rotated around the beam axis in the beam line.  
381 Advantages to the last two are that results are obtained over a somewhat larger area of the  
382 electrode, effects of preferred orientation in powder-containing electrodes are minimized, and  
383 counting statistics are improved.

384 Transmission XRD ring patterns (see Figure 2, step 5) can be obtained in about 10 seconds, with  
385 a data readout time of about 1-2 minutes. Integration of calibrated image patterns yields line  
386 scans (intensity vs. Q). Beam line 11-3 at the Stanford Synchrotron Radiation Lightsource uses a  
387 single Si(311) monochromator, generating an incident wavelength of approximately 0.97 Å  
388 (12,735 eV), though energy fluctuations **on the order of a few eVs (~0.01%) due primarily to**

389 diurnal cycling (daily temperature fluctuations) are often observed over the course of the lengthy  
390 charge and discharge measurements. Thus, image calibration for each scan is essential to de-  
391 convolute the diffraction pattern changes. Calibration is performed with The Area Diffraction  
392 Machine software developed in conjunction with the 11-3 beam line  
393 (<http://code.google.com/p/areadiffractionmachine/>).

394  
395 Figure 3 shows *in situ* XRD data obtained on a  $\text{Li/Li}_x[\text{Ni}_{0.45}\text{Mn}_{0.45}\text{Co}_{0.05}\text{Al}_{0.05}]\text{O}_2$  cell which  
396 underwent charge (in black) and discharge (in green), after calibration and conversion of the ring  
397 patterns to line scans. Peaks arising from cell components including the Al current collector,  
398 polyester pouch, and polypropylene separator are marked with red and blue dots (lithium metal is  
399 essentially transparent to x-rays, but additional peaks will arise if sodium metal anodes are used).  
400 Indexed reflections attributable to the  $\text{Li}_x[\text{Ni}_{0.45}\text{Mn}_{0.45}\text{Co}_{0.05}\text{Al}_{0.05}]\text{O}_2$  active material are marked  
401 on the patterns. Because the unit cell parameters changed as a function of x (Li content), peaks  
402 due to this phase and the Al current collector overlapped in some of the patterns. The  
403 interference from cell components presented significant challenges both for perfect background  
404 subtraction and Rietveld refinement of the entire diffraction patterns. To circumvent this  
405 problem, backgrounds were manually subtracted, and a limited set of peaks that did not overlap  
406 with cell components were selected for the fitting. Unit cell parameters at various states-of-  
407 charge were subsequently calculated by a least-squares refinement using the available peak  
408 positions and the program CelRef (<http://www.ccp14.ac.uk/tutorial/lmgp/celref.htm>). The degree  
409 to which cell components interfere in patterns obtained from *in situ* experiments vary depending  
410 on the nature of the material under study, and these problems are not always encountered. In that  
411 case, any convenient refinement or fitting program may be used to analyze data (GSAS,  
412 PowderCell, RIQAS, FullProf, etc.).

413 Due to time constraints, it is sometimes preferable to perform synchrotron XRD experiments *ex*  
414 *situ*. It is obviously not practical to perform multiple cycles over a long time in the beam line, for  
415 example. Instead, electrodes can be removed from cycled cells, rinsed with solvent to remove  
416 residual electrolyte salt, dried, and covered with Kapton film to provide protection from air, for  
417 later examination. Additionally, it can be useful to study a few electrodes at different states-of-  
418 charge harvested from electrochemical cells, to give an idea of what to expect from a more  
419 involved *in situ* experiment performed later. These experiments are much simpler to carry out  
420 and much less time-consuming; several samples can usually be run in an hour. An additional  
421 benefit to the *ex situ* work is the absence of most interfering cell components, although signals  
422 from the current collector, binder and conductive additives are usually still observed and the  
423 Kapton itself contributes to the background. **Caveats for *ex situ* work are that washing and long  
424 or improper storage may change or degrade the sample. In worst-case scenarios, the data  
425 obtained *ex situ* may not even provide relevant information because of these problems. If  
426 appropriate caution is maintained, however, *ex situ* work can still be of some value, although  
427 direct observation of processes using *in situ* configurations is clearly the most desirable option  
428 whenever time constraints allow.**

429 Because XAS experiments are element-specific, interference from cell components other than  
430 the electrode material of interest are not as problematic as with XRD (**assuming that cell  
431 hardware does not contain the metals of interest**). Only one absorption edge (element) can be  
432 measured at a time, however. **While switching to a new energy takes only seconds, tuning,  
433 changing gains and offsets on the ion chambers, changing reference foils, and purging with gas**

434 may take up to an additional ten minutes. Switching from one element to another during an *in*  
435 *situ* run may result in some loss of data. Meaningful EXAFS data can be difficult to obtain  
436 during *in situ* work, because the structural changes that are occurring often have similar time  
437 constants to that of the measurements themselves. Another consideration is that XAS beam lines  
438 are often heavily subscribed, meaning limited time for each user. For these reasons, it is  
439 generally more practical to carry out XAS experiments on *ex situ* samples rather than perform *in*  
440 *situ* work (although see reference 7 for an example of *in situ* work). Obtaining data on *ex situ*  
441 samples can take anywhere from a few minutes to one hour depending on how many elements  
442 are being studied and the facility at which the work is carried out. During each edge  
443 measurement, a similar metal foil (e.g., Ni, Mn, or Co) spectrum should be recorded for energy  
444 reference. This is carried out simultaneously with the sample measurement. In addition, the user  
445 may wish to record data on reference materials containing the metals of interest with known  
446 oxidation states, separately, particularly if unusual redox states are involved in the  
447 electrochemistry. For example,  $\text{Li}_3\text{MnO}_4$  was used as a reference for a recent study of a series of  
448 lithium manganese oxynitride electrode materials to verify the presence of tetrahedrally  
449 coordinated  $\text{Mn}^{5+}$ .

450 Most XAS experiments directed towards studying bulk processes in electrode materials are run  
451 in transmission mode, which is suitable when molar concentrations of the elements of interest are  
452 above about 5-10 % (<http://xafstraining.ps.bnl.gov>). Best results are obtained when the thickness  
453 of the sample,  $x$ , is adjusted so that  $\mu x < 3$  above the absorption edge. If the absorption coefficient  
454 ( $\mu$ ) is not known (e.g., for complex materials, which includes many battery electrode materials),  
455 it can be useful to start with a very small amount of powder sprinkled onto the sticky side of a  
456 piece of scotch tape. One or more additional pieces of powdered scotch tape can be attached to  
457 the original to increase the signal to the point where the optimum response is obtained (typically,  
458 corresponding to one absorption length). For materials where the absorption coefficient is  
459 known, the sample can be diluted with BN so that the correct absorption is obtained at a given  
460 thickness.

461 At SSRL, Ni, Mn, and Co K-edges can be studied at beam line 4.1, while Ti and S edges are  
462 investigated at beam line 4.3. Detuning the double crystal monochromator by about 30%  
463 eliminates higher order harmonics. Calibration is carried out using the first peak in the derivative  
464 of the absorption spectra of the reference metals. Duplicate scans can be run and merged after  
465 alignment to improve the quality of the data. Artemis/Athena from the software package  
466 IFEFFIT are used for analysis.<sup>9</sup> After merging like-scans, the background contribution is  
467 subtracted and the data is normalized. EXAFS data is isolated using the AUTOBK function, and  
468 is Fourier transformed. Least squares fitting to the Fourier transformed spectrum in R or k space  
469 is then used to extract structural information. An example of XAS data, taken at the Mn K edge,  
470 is shown in Figure 2, step 5 and the XANES and EXAFS regions are marked on the spectrum.

#### 471 **Tables and Figures:**

472 Figure 1: Schematic of a Li ion battery with a graphite anode and layered metal oxide cathode  
473 undergoing discharge. Used with permission from reference 4.

474 Figure 2: Typical sequence of an *in situ* experiment. Steps include 1) preparation and  
475 characterization of the sample, 2) preparation of composite electrodes, 3) assembly of pouch  
476 cells, 4) set up of an *in situ* experiment in the beamline, and 5) data acquisition and analysis.

477 Figure 3: Line scans obtained by integrating image scans on a  $\text{Li/Li}_x[\text{Ni}_{0.45}\text{Mn}_{0.45}\text{Co}_{0.05}\text{Al}_{0.05}]\text{O}_2$   
478 cell undergoing charge (black) and discharge (green). Reflections attributed to the Al current  
479 collector and polymeric cell components (pouch and microporous separator) are marked with  
480 blue and red dots, respectively.

481 Table 1: Table of Materials.

482 Table 2: Table of Equipment.

### 483 Discussion

484 Analysis of XANES data indicates that as-made  $\text{LiNi}_x\text{Co}_{1-2x}\text{Mn}_x\text{O}_2$  ( $0.01 \leq x \leq 1$ ) compounds  
485 contains  $\text{Ni}^{2+}$ ,  $\text{Co}^{3+}$ , and  $\text{Mn}^{4+}$ .<sup>10</sup> A recent *in situ* XAS study on  $\text{LiNi}_{0.4}\text{Co}_{0.15}\text{Al}_{0.05}\text{Mn}_{0.4}\text{O}_2$   
486 showed that  $\text{Ni}^{2+}$  was oxidized to  $\text{Ni}^{3+}$  and, ultimately,  $\text{Ni}^{4+}$  during delithiation, but that redox  
487 processes involving  $\text{Co}^{3+}$  contributed some capacity even at low states-of-charge, contrary to  
488 previous assumptions.<sup>7</sup> Another study involving the low cobalt compositions,  $\text{LiNi}_{0.45}\text{Co}_{0.1-}$   
489  $y\text{Al}_y\text{Mn}_{0.45}\text{O}_2$ , also indicated that Co was electroactive at the early stages of delithiation.<sup>11</sup>

490 Synchrotron XRD<sup>12</sup> and XAS<sup>11</sup> studies of a series of NMCs with the composition  
491  $\text{LiNi}_{0.45}\text{Mn}_{0.45}\text{Co}_{0.1-y}\text{Al}_y\text{O}_2$  ( $0 \leq y \leq 0.1$ ) have yielded insights into the improved electrochemical  
492 performance of the Al-substituted variants. Analysis of high-resolution synchrotron XRD  
493 patterns obtained on the pristine powders indicated that the  $y=0.1$  material exhibits a slight  
494 monoclinic distortion, not discernible in the conventional powder XRD patterns. To relieve strain  
495 in the transition metal planes, which consist of metal-containing edge-shared octahedra with  
496 different equilibrium M-O distances, local scale ordering occurs, resulting in the distortion. The  
497 strain-relieving distortion was further confirmed by close examination of the EXAFS data.<sup>11</sup>  
498 Electrochemical cycling induces additional strain, though the observed changes in the EXAFS  
499 data were smaller for electrodes containing Al. *In situ* XRD experiments on Li cells containing  
500 these NMC cathodes indicated that lattice changes during cell charge (delithiation) were smaller  
501 for the Al-substituted materials than for the unsubstituted baseline. Fewer structural changes  
502 upon prolonged cycling were also observed in the Al-containing electrodes.

503 Partial Al-substitution has also been proposed as a possible means to stabilize orthorhombic  
504  $\text{LiMnO}_2$  electrodes.<sup>13</sup> This material rapidly converts from the original zigzag layered structure to  
505 spinel upon electrochemical cycling, with a concomitant deterioration of the electrochemical  
506 properties. However, no stabilization effect was observed during *in situ* XRD experiments on an  
507 electrode substituted with 25% Al; in fact, reflections attributable to spinel formation were  
508 observed even during the initial cell charge.<sup>14</sup>

509 The degree of transition metal ordering in the high voltage spinel with the nominal composition  
510  $\text{LiNi}_{0.5}\text{Mn}_{1.5}\text{O}_4$  is expected to affect the voltage profile and other electrochemical characteristics  
511 of the material in operating cells.<sup>15</sup> In ordered materials (space group  $P4_332$ ), the Ni and Mn  
512 occupy  $4a$  and  $12d$  octahedral sites, respectively, whereas in the disordered variants (space group  
513  $Fd\bar{3}m$ ) the transition metals are distributed randomly over octahedral  $16d$  sites. A comparison  
514 of synchrotron xrd patterns obtained on two samples with differing degrees of transition metal  
515 ordering in an *in situ* experiment revealed very different phase behavior during delithiation  
516 processes.<sup>16</sup> The disordered material exhibited a wide solid solution region during the initial  
517 delithiation, with two narrow two-phase regions observed at high states-of-charge. The solid

518 solution region was much smaller for the ordered material, and the co-existence of three phases  
519 was observed at a composition of about  $x=0.3$  in  $\text{Li}_x\text{Ni}_{0.5}\text{Mn}_{1.5}\text{O}_4$ , flanked by two small two-  
520 phase regions. The dissimilarities in the phase behaviors, which are thought to be due to  
521 variations in lithium-vacancy ordering schemes, have been proposed as an explanation for rate  
522 capability differences observed between ordered and disordered  $\text{LiNi}_{0.5}\text{Mn}_{1.5}\text{O}_4$ . Contrary to  
523 expectations, however, the more ordered material in reference 16 performed better in this regard  
524 than the disordered sample. This was attributed to morphology effects; particles of the disordered  
525 sample consisted of plates with exposed (112) facets, whereas those of the ordered material were  
526 octahedral with (111) surface facets.

527 In addition to ordering and morphology effects, the physical and electrochemical characteristics  
528 of  $\text{LiNi}_{0.5}\text{Mn}_{1.5}\text{O}_4$  are also dependent on impurity content and the amount of  $\text{Mn}^{3+}$  present.  
529 During the high temperature processing used during synthesis, a Ni-containing rock salt impurity  
530 is formed and some  $\text{Mn}^{4+}$  is reduced to  $\text{Mn}^{3+}$  in the main phase. It can be difficult to detect small  
531 amounts of the rock salt impurity because of peak overlap in the XRD patterns, or to determine  
532 its exact composition, which varies with the thermal treatment. Analysis of Ni and Mn K edge  
533 XANES data revealed the presence of a significant amount of rock salt impurity containing both  
534 Ni and Mn in a sample made at  $1000^\circ\text{C}$ .<sup>17</sup>

535 The techniques described here were directed towards understanding bulk processes in electrodes  
536 undergoing charge and discharge. The assumption is that the structural changes observed using  
537 the very small spot size (e.g.,  $0.15 \times 0.15$  mm at beam line 11-3) for the experiment are typical of  
538 the electrode as a whole. This is generally true for well-made electrodes and cells, using the low  
539 current densities and relatively long charge-discharge times described above. *Ex situ* results have  
540 also generally been obtained on electrodes in cells subjected to normal operation, which have  
541 then undergone equilibration. In some circumstances, however, it can be instructive to obtain  
542 results under non-equilibrium conditions to gain understanding of failure modes of battery  
543 electrodes during operation at high current densities or under various abuse conditions. Non-  
544 uniform charge distributions may occur in these situations, particularly if electrodes or cells are  
545 unoptimized. The non-uniformity may result in local areas of overcharge or -discharge, causing  
546 structural degradation that ultimately results in reduced performance and safety of the device. A  
547 synchrotron x-ray microdiffraction technique has recently been used to map charge distribution  
548 in  $\text{LiFePO}_4$  electrodes charged at high rates.<sup>18</sup> Although this was performed *ex situ*, the two-  
549 phase nature of the  $\text{LiFePO}_4$  redox reaction essentially prevented relaxation of the charge  
550 distribution once the current was interrupted. For this experiment, partially charged electrodes  
551 were step-scanned using a monochromatic (6.02 keV) X-ray beam and a diffraction pattern was  
552 collected for each step. Scanning was carried out both perpendicular and parallel to the current  
553 collector on electrodes taken from partially charged coin cells and prismatic cells. In both cases,  
554 unequal distribution of charge was observed, with the surface of coin cell electrodes more highly  
555 charged than the active material close to the current collector, and the portion closest to the tab  
556 the most highly charged for the electrode taken from the prismatic cell.

557 These results illustrate the importance of good spatial as well as temporal resolution in  
558 synchrotron experiments directed towards a full understanding of battery operation. As the field  
559 advances, new techniques geared to imaging electrode materials in 3D are being developed. One  
560 such example is the combined use of full-field x-ray microscopy (TXM) with XANES to follow  
561 chemical and morphological changes in NiO electrodes as they underwent conversion to Ni and

562 Li<sub>2</sub>O during cell discharge.<sup>19</sup> A particular challenge for these experiments, however, can be  
563 handling the large amount of data that is generated.

564 New high throughput inelastic X-ray scattering configurations have also been used recently to  
565 obtain finer detail on the functioning of battery materials. Examples include a combined soft  
566 XAS (Fe L-edge) and hard X-ray Raman scattering study of LiFePO<sub>4</sub> electrodes, done *ex situ*.<sup>20</sup>  
567 The latter combines the advantages of a hard x-ray technique (e.g., ability to probe bulk  
568 phenomena and, eventually, to perform experiments *in situ* under a variety of conditions) with  
569 the sensitivity associated with soft x-ray XAS, and can be used for low z elements such as C and  
570 O.<sup>21</sup> Nonresonant inelastic x-ray scattering (NIXS) has also been used to measure the Li and O  
571 K-edges of Li<sub>2</sub>O<sub>2</sub> (the discharge product of lithium/air batteries with organic electrolytes),  
572 resulting in a better understanding of its structure.<sup>22</sup> The sensitivity of NIXS lends it particularly  
573 well for situations where poorly crystalline materials are encountered (such as in batteries  
574 undergoing discharge).

## 575 **Disclosures**

576 Authors have nothing to disclose.

## 577 **Acknowledgments**

578 This work is supported by the Assistant Secretary for Energy Efficiency and Renewable Energy,  
579 Office of Vehicle Technologies of the U.S. Department of Energy under Contract No. DE-AC02-  
580 05CH11231. Portions of this research were carried out at the Stanford Synchrotron Radiation  
581 Lightsource, a Directorate of SLAC National Accelerator Laboratory and an Office of Science  
582 User Facility operated for the U.S. Department of Energy Office of Science by Stanford  
583 University. The SSRL Structural Molecular Biology Program is supported by the DOE Office of  
584 Biological and Environmental Research, and by the National Institutes of Health, National  
585 Center for Research Resources, Biomedical Technology Program (P41RR001209).

## **References:**

1. Kim, S.-W., Seo, D.-I., Ma, X., Ceder G., Kang, K. Electrode Materials for Rechargeable Sodium-Ion Batteries: Potential Alternatives to Current Lithium-Ion Batteries. *Adv. Energy Mater.* 2 (2012): 710-721
2. Palomares, V., Serras, P., Villaluenga, I. Huesa, K. B., Cereitero-Gonzalez, J., Rojo, T. Na-ion Batteries, Recent Advances and Present Challenges to Become Low Cost Energy Storage Systems. *Energy & Environmental Science* 5 (2012): 5884 - 5901
3. Kam, K. C., Doeff, M. M., Electrode Materials for Lithium Ion Batteries. *Materials Matters.* 7 (2012): 56-60
4. Cabana, J., Monconduit, L., Larcher, D., Palacin, M.R., Beyond Intercalation-Based Li-Ion Batteries: The State of the Art and Challenges of Electrode Materials Reacting Through Conversion Reactions. *Adv. Energy Mater.* 22 (2010): E170-E192

5. McBreen, J., The Application of Synchrotron Techniques to the Study of Lithium Ion Batteries. *J. Solid State Electrochem.* 13 (2009): 1051-1061
6. de Groot, F., Vankó, G., Glatzel, P., The 1s X-ray Absorption Pre-edge Structures in Transition Metal Oxides. *J. Phys.:Condens. Matter* 21 (2009): 104207
7. Rumble, C., Conry, T. E., Doeff, M., Cairns, E. J., Penner-Hahn, J.E., Deb, A., Structural and Electrochemical Investigation of  $\text{Li}(\text{Ni}_{0.4}\text{Co}_{0.15}\text{Al}_{0.05}\text{Mn}_{0.4})\text{O}_2$ . *J. Electrochem Soc.* 157 (2010): A1317-A1322
8. Cabana, J., Dupré, N., Gillot, F., Chadwick, A.V., Grey, C.P., Palacín, M.R., Synthesis, Short-Range Structure and Electrochemical Properties of New Phases in the Li-Mn-N-O System. *Inorg. Chem.* 48 (2009): 5141-5153
9. Ravel, B., Newville, M., ATHENA, ARTEMIS, HEPHAESTUS: data analysis for X-ray absorption spectroscopy using IFEFFIT. *Journal of Synchrotron Radiation* 12 (2005): 537-541
10. Zeng D., Cabana, J. Bréger, Yoon, W.-S., Grey, C. P., *Chem. Mater.* 19 (2007): 6277-6289
11. Conry, T.E., Mehta, A., Cabana, J. Doeff, M. M., XAFS Investigation of  $\text{LiNi}_{0.45}\text{Mn}_{0.45}\text{Co}_{0.1-y}\text{Al}_y\text{O}_2$  Positive Electrode Materials. *J. Electrochem Soc.* 159 (2012): A1562-A1571
12. Conry, T.E., Mehta, A., Cabana, J., Doeff, M.M., Structural Underpinnings of the Enhanced Cycling Stability upon Al-substitution in  $\text{LiNi}_{0.45}\text{Mn}_{0.45}\text{Co}_{0.1-y}\text{Al}_y\text{O}_2$  Positive Electrode Materials for Li-ion Batteries. *Chem. Mater.* 24 (2012): 3307-3317
13. Reed, J., Ceder, G., Role of Electronic Structure in the Susceptibility of Metastable Transition-Metal Oxide Structures to Transformation. *Chem. Rev.* 104 (2004): 4513-4534
14. Cook, J. B., Kim, C., Xu, L., Cabana, J. The Effect of Al Substitution on the Chemical and Electrochemical Phase Stability of Orthorhombic  $\text{LiMnO}_2$ . *J. Electrochem. Soc.* 160 (2013): A46-A52
15. Lee, E., Persson, K., Revealing the Coupled Cation Interactions Behind the Electrochemical Profile of  $\text{Li}_x\text{Ni}_{0.5}\text{Mn}_{1.5}\text{O}_4$ . *Energy & Environ. Sci.* 5 (2012): 6047-6051
16. Hai, B., Shukla, A.K., Duncan, H., Chen, G., The Effect of Particle Surface Facets on the Kinetic Properties of  $\text{LiMn}_{1.5}\text{Ni}_{0.5}\text{O}_4$  Cathode Materials. *J. Mater. Chem. A* 1 (2013): 759-769
17. Cabana, J. et al., Composition-Structure Relationships in the Li-Ion Battery Electrode Material  $\text{LiNi}_{0.5}\text{Mn}_{1.5}\text{O}_4$ . *Chem. Mater.* 24 (2012): 2952-2964
18. Liu, J., Kunz M., Chen, K., Tamura, N., Richardson, T. J., Visualization of Charge Distribution in a Lithium Battery Electrode. *J. Phys. Chem. Lett.* 1 (2010): 2120-2123
19. Meirer, F., Cabana, J., Liu, Y., Mehta, A., Andrews, J. C., Pianetta, P., Three-dimensional Imaging of Chemical Phase Transformation at the Nanoscale with Full-Field Transmission X-ray Microscopy. *J. Synchrotron Rad.* 18 (2011): 773-781

20. Liu, X. et al., Phase Transformation and Lithiation Effect on Electronic Structure of  $\text{Li}_x\text{FePO}_4$ : An In-Depth Study by Soft X-ray and Simulations. *J. Am. Chem. Soc.* 134 (2012): 13708-13715

21. Sokaras, D. et al., A High Resolution and Solid Angle X-ray Raman Spectroscopy End-Station at the Stanford Synchrotron Radiation Lightsource. *Rev. Sci. Instrum.* 83 (2012): 043112

22. Chan, M.K. Y. et al., Structure of Lithium Peroxide. *J. Phys. Chem. Lett.* 2 (2011): 2483-2486

Table 1.

Name of Reagent/Material	Company	Catalog Number	Comments
Electrode active materials	Various		Synthesized in-house or obtained from various suppliers
Synthetic flake graphite	<a href="http://www.timcal.com">Timcal (www.timcal.com)</a>	SFG-6	Conductive additive for electrodes
Acetylene black	<a href="http://www.denka.co.jp/eng/index.html">Denka (http://www.denka.co.jp/eng/index.html)</a>	Denka Black	Conductive additive for electrodes
1-methyl-2-pyrrolidinone (NMP)	Sigma-Aldrich ( <a href="http://www.sigmaaldrich.com">www.sigmaaldrich.com</a> )	328634	Used to make electrode slurries
Al current collectors	<a href="http://www.exopackadvancedcoatings.com">Exopack (http://www.exopackadvancedcoatings.com)</a>	z-flo 2650	Carbon-coated foils. Coated on one side.
	Alfa-Aesar ( <a href="http://www.alfa.com">http://www.alfa.com</a> )	10558	0.025mm (0.001in) thick, 30x30cm (12x12in), 99.45% (metals basis), uncoated
Cu current collectors	<a href="http://www.predmaterials.com">Pred Materials (www.predmaterials.com)</a>	Electrodeposited Cu foil	For use with anode materials for Li ion batteries.

Lithium foil	<a href="http://www.rockwoodlithium.com">Rockwood Lithium (www.rockwoodlithium.com)</a>	Contact vendor	Anode for half cells. Available in different thicknesses and widths. Reactive and air sensitive. Store and handle in an inert atmosphere glovebox under He or Ar (reacts with N <sub>2</sub> ).
Sodium ingot	<a href="http://www.sigmaaldrich.com">Sigma-Aldrich (www.sigmaaldrich.com)</a>	320080	Anodes for half cells. Can be extruded into foils. Reactive and air sensitive. Store and handle in an inert atmosphere glovebox under He only.
Electrolyte solutions	<a href="http://www.catalysts.basf.com/p02/USWeb-Internet/catalysts/en/content/microsites/catalysts/prods-inds/batt-mats/electrolytes">BASF (http://www.catalysts.basf.com/p02/USWeb-Internet/catalysts/en/content/microsites/catalysts/prods-inds/batt-mats/electrolytes)</a>	Selectilyte P-Series contact vendor	Contact vendor for desired formulations.
Dimethyl carbonate (DMC)	<a href="http://www.sigmaaldrich.com">Sigma-Aldrich (www.sigmaaldrich.com)</a>	517127	Used to wash electrodes for <i>ex situ</i> experiments.
Microporous separators	<a href="http://www.celgard.com">Celgard (http://www.celgard.com)</a>	2400	Polypropylene membranes
Coin cell hardware (case, cap, gasket)	<a href="http://www.predmaterials.com">Pred Materials (www.predmaterials.com)</a>	CR2016, CR2025, CR2320, CR2032	Match size to available crimping tool, Al-clad components also available.

Wave washers	<a href="http://www.predmaterials.com">Pred Materials (www.predmaterials.com)</a>	SUS316L	
Spacers	<a href="http://www.predmaterials.com">Pred Materials (www.predmaterials.com)</a>	SUS316L	
Ni and Al pre-taped tabs	<a href="http://www.predmaterials.com">Pred Materials (www.predmaterials.com)</a>	Contact vendor	Sizes subject to change. Inquire about custom orders.
Polyester pouches	VWR ( <a href="https://us.vwr.com">https://us.vwr.com</a> )	11214-301	Used to seal electrochemical cells for <i>in situ</i> work. Avoid heavy duty pouches because of strong signal interference.
Kapton film	<a href="http://www.mcmaster.com">McMaster-Carr (www.mcmaster.com)</a>	7648A735	Used to cover electrodes for <i>ex situ</i> experiments, 0.0025" thick
Helium, Argon and 4-10% hydrogen in helium or argon	Air Products ( <a href="http://www.airproducts.com/products/gases.aspx">http://www.airproducts.com/products/gases.aspx</a> )  or any other suitable gas supplier	contact vendor for desired compositions and purity levels  Purity level needed depends on whether the glovebox is equipped with a water and oxygen removal system. Hydrogen mixtures	Helium or argon used to fill glovebox where cell assembly is carried out and alkali metal is stored.  Do not use nitrogen because it reacts with lithium. Use only helium if sodium is being stored.

needed to  
regenerate  
water/oxygen  
removal system, if  
present

Table 2.

Name of Equipment	Company	Catalog Number	Comments
Inert atmosphere glovebox	Vacuum Atmospheres ( <a href="http://vac-atm.com">http://vac-atm.com</a> )	Custom order, contact vendors	used during cell assembly and to store alkali metals and moisture sensitive components
	Mbraun ( <a href="http://www.mbraunusa.com">http://www.mbraunusa.com</a> )		various sizes (single, double) available, many options such as mini or heated antechambers  oxygen/water removal systems, shelving, electrical feedthroughs, etc.
X-ray powder Diffractometer (XRD)	Panalytical ( <a href="http://www.panalytical.com">www.panalytical.com</a> )	X'Pert Powder	X'Pert is a modular system. Many accessories available for specialized experiments.
	Bruker ( <a href="http://www.bruker.com">www.bruker.com</a> )	Bruker D2 Phaser	Bruker D2 Phaser is compact and good for routine powder analyses.
Scanning Electron Microscope (SEM)	JEOL ( <a href="http://www.jeolusa.com">http://www.jeolusa.com</a> )	JSM7500F	High resolution field emission scanning electron microscope with numerous customizable options.
		contact vendor for options	Low cost tabletop versions also available.
Pouch Sealer	<a href="https://us.vwr.com">VWR (https://us.vwr.com)</a>	11214-107	Used to seal pouches for <i>in situ</i> work
Manual crimping tool	<a href="#">Pred Materials</a>	HSICC-2016,	Used to seal coin cells. Match size to coin cell hardware

	<a href="http://www.predmaterials.com">www.predmaterials.com</a>	2025, 2032, 2320	
Coin cell disassembling tool	<a href="http://www.predmaterials.com">Pred Materials www.predmaterials.com</a>	Contact vendor	Used to take apart coin cells to recover electrodes for <i>ex situ</i> work. Needlenose pliers can also be used. Cover ends with Teflon tape to avoid shorting cells.
Film casting knives	<a href="https://www.byk.com">BYK Gardner https://www.byk.com</a>	4301, 4302, 4303, 4304, 4305, 2325, 2326, 2327, 2328, 2329	Used to cast electrodes films from slurries. Different sizes available, with either metric or English gradations. Bar film or Baker-type applicators and doctor blades are less versatile but lower cost options.
Doctor blades, Baker applicators	<a href="http://www.predmaterials.com">Pred Materials www.predmaterials.com</a>	Baker type applicator and doctor blade. Film casting knives also available.	Can be used by hand or with automatic film applicators.
Automatic film applicator	<a href="https://www.byk.com">BYK Gardner https://www.byk.com</a> <a href="http://www.predmaterials.com">Pred Materials www.predmaterials.com</a>	2101, 2105, 2121, 2122 Contact vendor	Optional. Used with bar applicators, doctor blades, or film casting knives for automatic electrode film production. Films can also be made by hand but are less uniform.
Potentiostat/Galvanostat	<a href="http://www.bio-logic.info">Bio-Logic Science Instruments http://www.bio-logic.info</a> Gamry Instruments (www.gamry.com)	VSP Reference 3000	Portable 5 channel computer-controlled potentiostat/galvanostat used to cycle cells for <i>in situ</i> experiments. Portable single channel computer-controlled potentiostat/galvanostat used to cycle cells for <i>in situ</i> experiments.

The Area Diffraction Machine	<a href="http://code.google.com/p/areadiffractionmachine/">http://code.google.com/p/areadiffractionmachine/</a>	Free download	Used for analysis of 2D diffraction data. Mac and Windows versions available.
IFEFFIT	<a href="http://cars9.uchicago.edu/ifeffit/">http://cars9.uchicago.edu/ifeffit/</a>	Free download	Suite of interactive programs for XAS analysis, including Hephaestus, Athena, and Artemis. Available for Mac, Windows, and UNIX.
SIXPACK	<a href="http://home.comcast.net/~sam_webb/sixpack.html">http://home.comcast.net/~sam_webb/sixpack.html</a>	Free download	XAS analysis program that builds on IFEFFIT. Windows and Mac versions.
CelRef	<a href="http://www.ccp14.ac.uk/tutorial/lmgp/celref.htm">http://www.ccp14.ac.uk/tutorial/lmgp/celref.htm</a> and <a href="http://www.ccp14.ac.uk/ccp/web-mirrors/lmgp-laugier-bochu/">http://www.ccp14.ac.uk/ccp/web-mirrors/lmgp-laugier-bochu/</a>	Free download	Graphical unit cell refinement. Windows only.

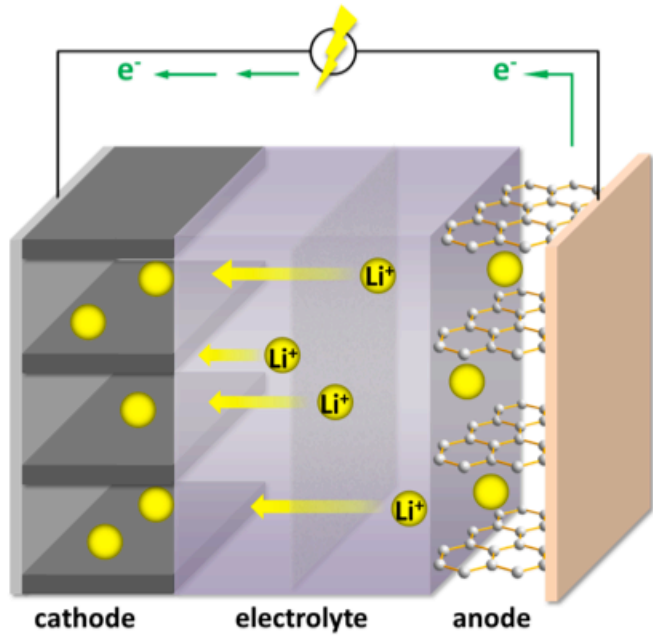
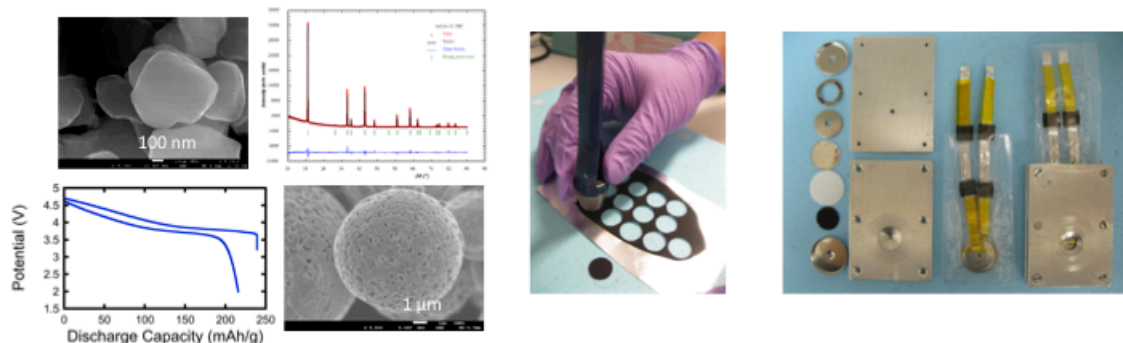
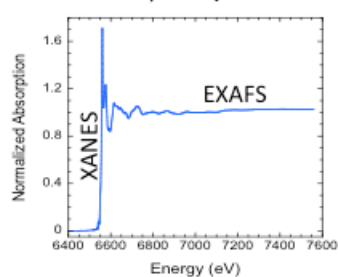


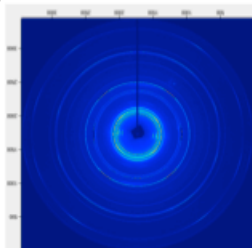
Figure 1



- 1) Prepare/characterize samples 2) Prepare electrodes 3) Assemble pouch cells  
 5) Acquire and analyze data ← 4) Run experiment in beam line



*Mn K-edge XAS data*



*2D diffraction image collected from area detector*



Figure 2

Figure 2

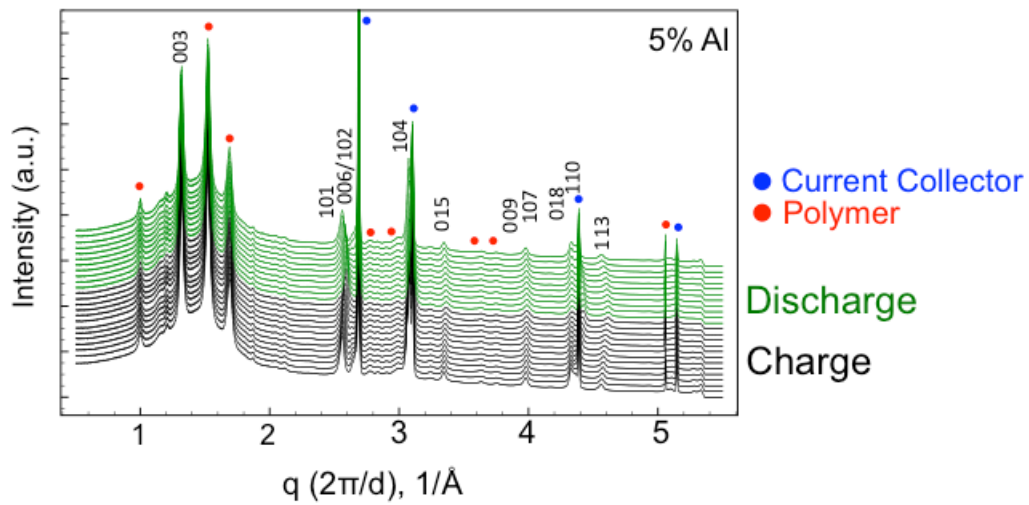


Figure 3

Figure 3